PHYSICAL REVIEW B **96**, 180415(R) (2017)

Dirac-surface-state-dominated spin to charge current conversion in the topological insulator $(Bi_{0.22}Sb_{0.78})_2Te_3$ films at room temperature

J. B. S. Mendes,[1,*] O. Alves Santos,[2] J. Holanda,[2] R. P. Loreto,[1] C. I. L. de Araujo,[1] Cui-Zu Chang,[3,4] J. S. Moodera,[3,5] A. Azevedo,[2] and S. M. Rezende[2]

[1]*Departamento de Física, Universidade Federal de Viçosa, 36570-900 Viçosa, MG, Brazil*

[2]*Departamento de Física, Universidade Federal de Pernambuco, 50670-901 Recife, PE, Brazil*

[3]*Francis Bitter Magnet Laboratory, Massachusetts Institute of Technology, Cambridge, Massachusetts 02139, USA*

[4]*Department of Physics, The Pennsylvania State University, University Park, Pennsylvania 16802, USA*

[5]*Department of Physics, Massachusetts Institute of Technology, Cambridge, Massachusetts 02139, USA*

(Received 16 August 2017; published 28 November 2017)

We report the spin-to-charge current conversion in an intrinsic topological insulator (TI) $(Bi_{0.22}Sb_{0.78})_2Te_3$ film at room temperature. The spin currents are generated in a thin layer of permalloy (Py) by two different processes, the spin pumping effect (SPE) and the spin Seebeck effect (SSE). In the first, we use microwave-driven ferromagnetic resonance of the Py film to generate a SPE spin current that is injected into the TI $(Bi_{0.22}Sb_{0.78})_2Te_3$ layer in direct contact with Py. In the second, we use the SSE in the longitudinal configuration in Py without contamination by the anomalous Nernst effect, which was made possible with a thin NiO layer between the Py and $(Bi_{0.22}Sb_{0.78})_2Te_3$ layers. The spin-to-charge current conversion is dominated by the TI surface states and is attributed to the inverse Edelstein effect (IEE), which is made possible by the spin-momentum locking in the electron Fermi contours due to the Rashba field. The measurements by the two techniques yield very similar values for the IEE parameter, which are larger than the reported values in the previous studies on topological insulators.

DOI: 10.1103/PhysRevB.96.180415

Topological insulators (TIs) constitute a novel state of matter, which have been the subject of intensive investigations in condensed matter physics in the last decade. They are a new class of quantum materials that present insulating bulk, but metallic, dissipationless surface states topologically protected by time reversal symmetry, opening several possibilities for practical applications in many scientific arenas including spintronics, quantum computation, magnetic monopoles, and highly correlated electron systems [1–4]. More recently, it has been shown that TI particles behave as optically induced oscillators in optical tweezers [5]. The surface states are characterized by a single gapless Dirac cone and exhibit remarkable spin-momentum locking: The charge carriers move in such a way that their momenta are always perpendicular to their spin [4,6]. In addition, topological insulators have strong spin-orbit coupling (SOC) and as well as have a large spin torque, which are essential for efficient spin-charge conversion [7–9].

In turn, the conversion of charge currents into spin currents, and vice versa, are key phenomena for encoding and decoding information carried by electron spins in the active field of spintronics. Until recently, the only known mechanisms for conversion in both directions were the spin Hall effect (SHE) and its Onsager reciprocal, the inverse spin Hall effect (ISHE), which rely on electron scattering processes with spin-orbit interactions in three-dimensional (3D) materials [10–14]. Studies of the spin-to-charge conversion by the ISHE have been conducted in metallic films with heavy elements, such as paramagnetic Pt, Pd, and Ta [15–27], ferromagnetic Py [28], antiferromagnetic materials such as IrMn and PtMn [29,30], and semiconductors [31–37]. Recent developments in thin-film growth techniques have made possible the fabrication of samples with atomically flat surfaces and interfaces that have led to the observation of new phenomena induced by SOC in two-dimensional (2D) systems [38–40]. Among them are the Edelstein effect, predicted some time ago [41], and its Onsager reciprocal, the inverse Edelstein effect, that enable new means to convert charge currents into spin currents, and vice versa.

The direct Edelstein effect and the inverse Edelstein effect (IEE) are made possible by the Rashba effect that arises from SOC and broken inversion symmetry at material surfaces and interfaces [42–45]. The Rashba field produces spin-momentum locking in the electron Fermi contours that enables the conversion between spin and charge currents. The conversion of spin currents produced by ferromagnetic resonance (FMR) spin pumping into charge currents due to the IEE has been observed at Bi/Ag interfaces [46], single-layer graphene [47], and in a few TIs [8,48–50]. In this Rapid Communication, we report the observation of spin-to-charge current conversion by means of the IEE in the topological insulator $(Bi_{0.22}Sb_{0.78})_2Te_3$ at room temperature. The spin currents are generated by two different arrangements, microwave-driven spin pumping and the spin Seebeck effect.

The experiments were carried out with two sample structures, (i) one consisting of a TI grown on a 0.5-mm-thick sapphire (0001) substrate and with a $Ni_{81}Fe_{19}$ (permalloy-Py) top layer, and (ii) a trilayer in which a NiO layer is grown between the TI and the Py layers. In both, we have used a commercial 0.5-mm-thick (0001) sapphire substrate onto which the TI is grown as follows. After high-temperature annealing (~800 °C) of the sapphire substrate, a six-quintuple layer (QL)-thick $(Bi_xSb_{1-x})_2Te_3$ film is grown on top at a temperature ~230 °C in a custom-built ultrahigh vacuum molecular beam epitaxy (MBE) system and capped by a 3-nm-thick epitaxial Te layer. X-ray diffraction patterns confirm the

*Corresponding author: joaquim.mendes@ufv.br

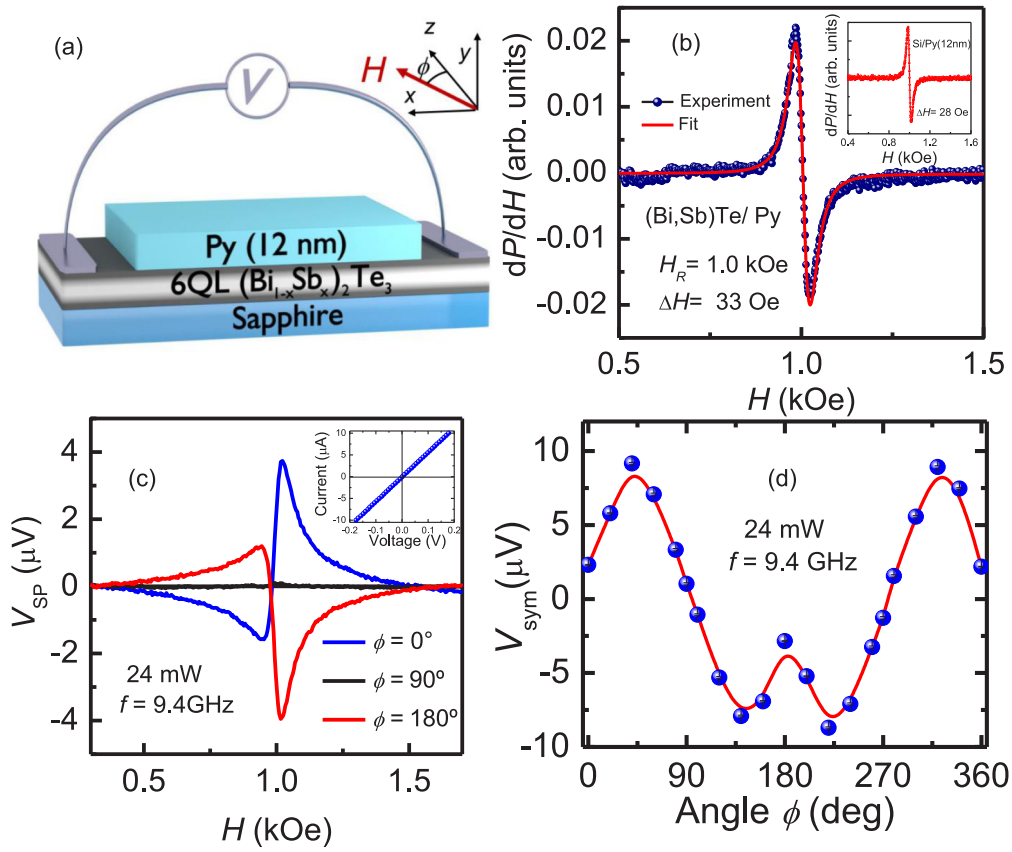

FIG. 1. (a) Sketch of the bilayer sample 6-QL $(Bi_{0.22}Sb_{0.78})_2Te_3$/Py(12 nm) and coordinate system, where ϕ is the in-plane angle. (b) FMR absorption derivative vs magnetic field H measured at 9.4 GHz and microwave power of 24 mW. The inset shows the FMR spectrum for a single Py (12 nm) layer on a Si substrate. (c) Voltage measured between the electrodes for three angles of the in-plane field, with the same microwave frequency and power as in (b). The inset shows the I-V curve of the $(Bi_{0.22}Sb_{0.78})_2Te_3$/Py structure demonstrating the formation of Ohmic contacts between the electrodes. (d) Angular dependence of the symmetric (peak) component of the voltage line. The experimental data are represented by the solid circle symbols and the theoretical fit by the solid curve.

high crystalline, single phase quality of the films, with growth along the c axis [see the Supplemental Material for more details about the conditions of growth and the crystallographic structure of the $(Bi_{0.22}Sb_{0.78})_2Te_3$ films [51]]. We have chosen a Bi concentration $x = 0.22$ to locate the Fermi level close to the Dirac point [52–54]. The Py layer is deposited by dc magnetron sputtering, either directly on the TI film or separated by an insulating NiO layer, grown by rf sputtering at 160 °C. The Py and NiO films were deposited in a 3 mTorr argon atmosphere in the sputter-up configuration, with the substrate at a distance of 9 cm from the target, and with a deposition rate fixed in 1 and 0.3 Å/s, respectively. Therefore, the Py and NiO layers were gently deposited over the TI to minimize any detrimental effect on the surface chemistry. Finally, two silver electrodes were attached to the ends of the TI layer for measuring the induced voltages.

For the ferromagnetic resonance and spin pumping experiments the sample was mounted on the tip of a polyvinyl chloride (PVC) rod and inserted through a hole drilled in the center of the back wall of a rectangular microwave cavity operating in the transverse electric (TE_{102}) mode, at a frequency of 9.4 GHz with a Q factor of 2000. The sample is slightly inserted into the cavity in the plane of the back wall, in a position of maximum rf magnetic field and minimum rf electric field to avoid the generation of galvanic effects driven by the electric field. With this arrangement the static magnetic field H and the microwave field h_{rf} are in the film plane and kept perpendicular to each other as the sample is rotated for the measurements of the angular dependence of the FMR spectra and the dc voltage induced by the magnetization precession. Field scan spectra of the derivative of the microwave absorption dP/dH are obtained by modulating the field at 1.2 kHz and using lock-in detection. All FMR and voltage measurements were taken at room temperature.

Figure 1(a) shows a schematic illustration of the 6-QL $(Bi_{0.22}Sb_{0.78})_2Te_3$/Py (12 nm) bilayer sample used in the spin pumping effect (SPE) experiments, which has a length of 3 mm and a width of 1.5 mm. The Py films have in-plane magnetization, and thus the magnetic proximity effect is expected to shift the Dirac cone sideways along the momentum direction and does not open an exchange gap (i.e., in our heterostructures, the Dirac cone of the TI film will be preserved). Figure 1(b) shows the FMR absorption spectrum of the Py layer in contact with the TI film measured with a microwave power of 24 mW. The FMR line has the shape of a Lorentzian derivative with a peak-to-peak linewidth of 38.1 Oe, corresponding to a half width at half maximum

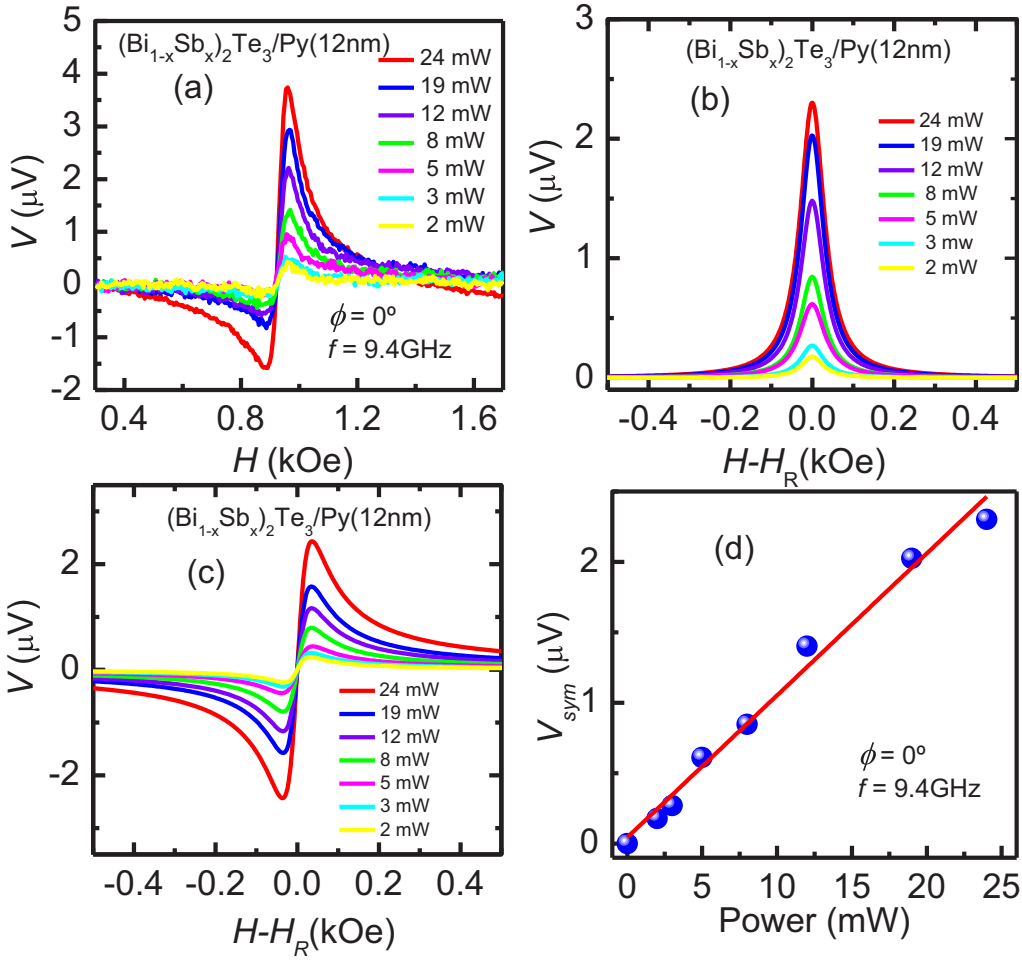

FIG. 2. (a) Voltage measured between the electrodes at the field angle $\phi = 0^\circ$ for several microwave power levels, as indicated. (b) and (c) Variation with power of the symmetric and antisymmetric components of the voltage obtained by the fitting of Lorentzian derivative functions to the line shapes in (a). (d) Power dependence of the measured symmetric peak component of the voltage at $\phi = 0^\circ$.

(HWHM) linewidth of $\Delta H = 33.0$ Oe. As shown in the inset of Fig. 1(b), an identical Py layer deposited on a Si substrate has a linewidth $\Delta H_{\rm Py} = 28.0$ Oe, showing that the contact of the TI layer produces an additional damping due to the spin pumping process [55,56], similar that observed in Pt/Py bilayers [17,19]. Figure 1(c) shows the field (H) scan dc voltage measured directly with a nanovoltmeter connected by copper wires to the electrodes, for a microwave power of 24 mW, for three angles of the in-plane field. For $\phi = 0^\circ$, the voltage line shape is the superposition of symmetric and antisymmetric components, changes sign with inversion of the field, and vanishes for the field along the sample strip $\phi = 90^\circ$.

The field dependence voltage $V(H)$ measured between the electrodes can be described by the sum of two components, $V(H) = V_{\rm sym} L(H - H_R) + V_{\rm asym} D(H - H_R)$, where $L(H - H_R)$ is the (symmetric) Lorentzian function and $D(H - H_R)$ is the (antisymmetric) Lorentzian derivative centered about the FMR resonance field H_R. The voltage line shape measured as function of the field angle ϕ can be fit with the expression

$$V(H,\phi) = V_Q^{\rm peak} L(H - H_R)\cos\phi + \left[V_{\rm CL}^{\rm sym} L(H - H_R) + V_{\rm CL}^{\rm asym} D(H - H_R)\right]\sin 2\phi \sin\phi, \quad (1)$$

where $V_{\rm CL}^{\rm sym}$ and $V_{\rm CL}^{\rm asym}$ denote the amplitudes of the symmetric and antisymmetric components of the classical contributions, such as the galvanic effect, or spin rectification, generated in the Py layer [19], and $V_Q^{\rm peak}$ is the peak value of the symmetric contribution to the voltage of quantum origin, which will be discussed later. Figure 1(d) shows the measured angle dependence of the symmetric component, which is the one of interest here, and a solid curve representing the fit obtained with Eq. (1).

Figure 2(a) shows the voltage line shapes measured at several power levels, and Figs. 2(b) and 2(c) show the corresponding symmetric and antisymmetric components of the line shapes, obtained by fitting the sum of a Lorentzian function and a Lorentzian derivative to the data. Figure 2(d) shows that the symmetric component at $\phi = 0^\circ$, which is $V_Q^{\rm peak}$, exhibits a linear dependence with the microwave power. From Figs. 1(d) and 2(b) we have the value for the voltage of quantum origin at $\phi = 0^\circ$, $V_Q^{\rm peak} = 2.3\,\mu$V, for a microwave power of 24 mW, part of which is due to the magnonic charge pumping (MCP) that is produced in a single Py layer [57]. In order to separate the contributions, we have measured the voltage induced in a single layer of Py(12 nm) on a Si substrate in the same conditions of the data in Figs. 1 and 2. For a microwave

power of 24 mW, the symmetric component at $\phi = 0$ has a peak value of 0.4 μV.

The most important source for the symmetric component of the voltage, and the one of interest here, is the conversion of the spin current produced by spin pumping into charge current in the TI layer. As is well known [12–19], in a ferromagnetic (FM) layer under ferromagnetic resonance, the precessing magnetization generates a spin current density (in units of charge/time area) at the FM/TI interface given by

$$J_S = \frac{e\omega p g_{\rm eff}^{\uparrow\downarrow}}{8\pi}\left(\frac{h_{\rm rf}}{\Delta H}\right)^2 L(H - H_R), \qquad (2)$$

where e is the electron charge, $g_{\rm eff}^{\uparrow\downarrow}$ is the real part of the effective spin mixing conductance at the interface that takes into account the spin-pumped and backflow spin currents [12–19,55,56], ω and $h_{\rm rf}$ are, respectively, the frequency and amplitude of the driving microwave magnetic field, and p is the precession ellipticity factor $p = 4(\omega/\gamma)(H_R + 4\pi M_{\rm eff})/(2H_R + 4\pi M_{\rm eff})^2$, where $4\pi M_{\rm eff}$ is the effective magnetization that appears in the expression for the FMR frequency $f = \gamma[H_R(H_R + 4\pi M_{\rm eff})]^{1/2}$. The spin current produced by the FMR spin pumping flows through the FM/TI interface into the TI layer. We follow Refs. [8,44–50] and interpret the spin-to-charge conversion in the TI layer as arising from the inverse Edelstein effect (IEE), which has its origin in the spin-momentum locking in the Fermi contours due to the Rashba SOC interaction. The 3D spin current in Eq. (2) flows into the TI layer and is converted by the IEE into a lateral charge current with a 2D density $j_C = (2e/\hbar)\lambda_{\rm IEE} J_S$, where $\lambda_{\rm IEE}$ is a coefficient characterizing the IEE, with the dimension of length and proportional to the Rashba coefficient, and hence to the magnitude of the SOC [8,44–46]. The measured voltage is related to this current density by $V_{\rm IEE} = R_S w j_C$, where R_S is the shunt resistance, w the width of the (Bi,Sb)Te/Py bilayer in the length of the Py layer, and j_C has units of A/m.

In order to obtain the IEE length from the experimental data, we need initially to calculate the SPE spin current. The real part of the spin mixing conductance of the (Bi,Sb)Te/Py interface that enters in Eq. (2) can be inferred from the broadening of the FMR linewidth due to the spin pumping process using $g_{\rm eff}^{\uparrow\downarrow} = (4\pi M_0 t_{\rm Py}/\hbar\omega)(\Delta H - \Delta H_{\rm Py})$ [12–14,17,55,56]. With $4\pi M_0 = 11$ kG, $t_{\rm Py} = 12$ nm, $\omega/2\pi = 9.4$ GHz, we find that the additional linewidth of 5 Oe measured in Py due to the contact with the TI layer corresponds to $g_{\rm eff}^{\uparrow\downarrow} = 1.0 \times 10^{19}$ m^{-2}, a value similar to the one for Py/Pt interfaces, demonstrating an efficient spin transfer in (Bi,Sb)Te/Py heterostructures [12–19]. The amplitude of the microwave field in Eq. (1), in Oe, is related to the incident power P_i, in W, by $h_{\rm rf} = 1.776(P_i)^{1/2}$, calculated for a microwave cavity made with a shorted standard X-band rectangular waveguide, operating in the TE_{102} mode with a Q factor of 2000, at a frequency of 9.4 GHz. Using these values, we obtain for $P_i = 24$ mW, $H = H_R$, the spin current density at the interface produced by the FMR spin pumping $J_S = 2.3 \times 10^5$ A/m^2. The charge current density due to the conversion from the spin current by the IEE, given by $j_C = V_{\rm IEE}^{\rm peak}/(wR_S)$, corresponding to the measured voltage of $V_{\rm IEE}^{\rm peak} = 1.9\,\mu$V, considering that the shunt resistance is approximately the one of the Py layer, $R_S = 71\,\Omega$, and

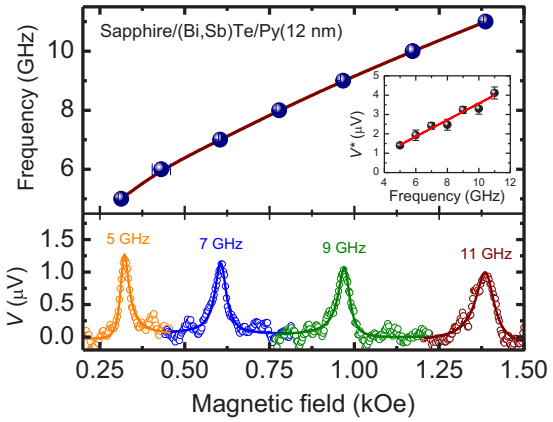

FIG. 3. Lower panel: Voltage measured between the electrodes on the TI strip at the field angle $\phi = 0°$ for several microwave driving frequencies, as indicated, and power 28 mW. Upper panel: Driving frequency vs the field value for the peak voltage. The inset shows the variation with frequency of the peak voltage normalized by the FMR linewidth squared referred to the value at 5 GHz.

$w = 1.5$ mm, is $j_C = 1.7 \times 10^{-5}$ A/m. Thus, the IEE length $\lambda_{\rm IEE} = j_C/J_S$ obtained from the spin pumping measurements is $\lambda_{\rm IEE} = 0.075$ nm. It is important to note that the magnitude of the IEE coefficient should depend not only on intrinsic TI properties, but also on sample preparation processes. In recent studies of TI-based spin pumping works, the interface property plays a critical role for enhancing the spin conversion efficiency [48,50]. Thus, structural defects in the fabrication of heterostructures can potentially result in the observed lower values for spin conversion efficiency. However, a detailed investigation of understanding about the correlation of the interfacial conditions of TI surfaces states and the spin-charge conversion efficiency would be desirable.

The spin pumping origin of the spin current pumped into the TI was confirmed by using a broadband microwave microstrip setup and measuring the voltage between the electrodes on the TI strip with scanning H for several frequencies, keeping constant the incident power at the $P_i = 28$ mW. With this power level, the rf magnetic field produced in the sample placed on a copper microstrip 0.5 mm wide, with a characteristic impedance $Z_0 = 50\,\Omega$, is very similar to the one in the microwave cavity with $Q = 2000$ with power 24 mW previously described. The field dependencies of the voltages measured at several frequencies are shown in the lower panel of Fig. 3 with Lorentzian fits. One clearly sees the broadening of the voltage lines with increasing frequency, which is a characteristic feature of the spin pumping damping [55,56]. The upper panel in Fig. 3 shows the variation of the measured field value for the peak voltage, that is, the FMR field H_R, with the driving frequency. In order to compare the voltages measured at the various frequencies we need to consider that the peak value of the pumped spin current varies inversely with the FMR linewidth squared ΔH^2, as in Eq. (2). Thus we introduce the normalized peak voltage, defined by $V^* = V(\Delta H/\Delta H_5)^2$, where V and ΔH are, respectively, the peak voltage and the linewidth measured at a frequency f, and ΔH_5 is the linewidth at 5 GHz. The linear increase of the normalized peak voltage shown in the inset of the upper panel

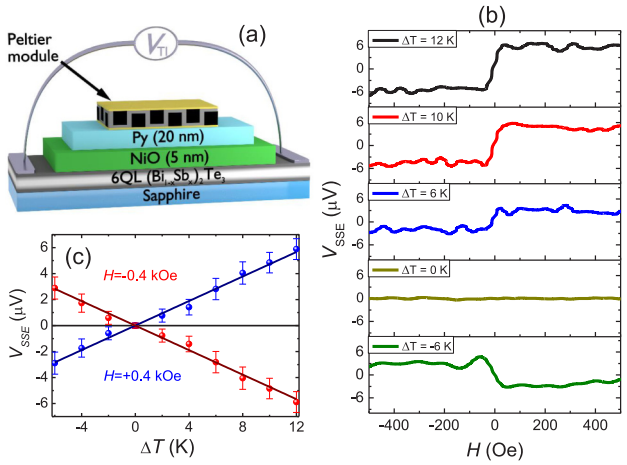

FIG. 4. (a) Schematic illustration of the sample 6-QL $(Bi_{0.22}Sb_{0.78})_2Te_3$/NiO/Py(12 nm) structure used to measure the voltages generated by the ANE and SSE. (b) Variation with magnetic field of the SSE-IEE voltage measured in the TI layer, created by the combined SSE in the Py layer and IEE in the TI, for several values of ΔT, as indicated. Positive ΔT corresponds to the Peltier module warmer than the substrate. (c) Variation with temperature difference of the SSE-IEE voltage measured with $H = 0.4$ kOe, in two field directions.

of Fig. 3 provides more evidence of the spin pumping origin of voltage induced in the TI layer.

In order to confirm the spin-to-charge current conversion in $(Bi_{1-x}Sb_x)_2Te_3$ by the IEE, we have used another process to generate spin currents, namely, the spin Seebeck effect (SSE). We used a sample arrangement illustrated Fig. 4(a), in which a 5-nm-thick NiO layer provides electrical isolation between the TI and Py films. The Py layer has a width of 1.0 mm, smaller than the NiO and TI layers, to avoid possible contacts at the edges. A commercial Peltier module, of width 4 mm, is used to heat or cool the side of the Py layer while the substrate is maintained in thermal contact with a copper block at room temperature. The temperature difference ΔT across the sample is calibrated as a function of the current in the Peltier module by means of a differential thermocouple. The temperature gradient perpendicular to the Py layer has two effects: One is to generate a voltage along the layer by means of the classical anomalous Nernst effect (ANE) [58–61]; the other is to generate a spin current across the Py layer by the longitudinal spin Seebeck effect (LSSE) [61–66]. Since NiO is a room-temperature antiferromagnet, it blocks the flow of charge current but transports spin currents [66–70], thus allowing measurements of the voltage generated in the TI layer separated from the voltage induced in the Py layer by the ANE. Figure 4(b) shows the voltages measured between the two electrodes in the $(Bi_{1-x}Sb_x)_2Te_3$ layer that are produced by the electric current resulting from the IEE spin-to-charge conversion of the spin current generated by the spin Seebeck effect in the Py layer that is injected into the Py/NiO interface and transported by the magnons in the NiO layer. The magnetic field dependencies of the SSE-IEE voltages in the TI layer for several values of the temperature difference ΔT across the sample structure are shown in Fig. 4(b). Note that $\Delta T > 0$ corresponds to the Peltier module warmer than the substrate. The data have the shape of the hysteresis curve of Py with very small coercitivity in the field scale of the measurements. The change in the voltage sign with the field reversal is due to the sign change of the spin polarization. Figure 4(c) shows the measured variation of the voltage plateau with the temperature difference ΔT for applied fields of $H = \pm 0.4$ kOe. The linear dependence of V_{SSE} on ΔT results from the fact that the spin current generated by the LSSE in Py is proportional to the temperature gradient across the Py layer [66]. In order to calculate the IEE parameter obtained from the SSE-IEE measurements, we use data for the SSE in Si/Py/NiO/Pt in Ref. [66] and rescale the numbers accordingly. The value of the charge current measured in the Pt layer in the sample Si/Py(20 nm)/NiO(5 nm)/Pt(6 nm) for $\Delta T = 12$ K is 24.3 nA, corresponding to a current density in the Pt layer of width 2.5 mm and thickness 6 nm of $J_C = 1.6 \times 10^3$ A/m^2 [66]. Considering for the spin Hall angle of Pt the value $\theta_{SH} = 0.05$ [12–14], this gives for the spin current density reaching the Pt after attenuation in the NiO layer the value $J_S = 3.2 \times 10^4$ A/m^2 for $\Delta T = 12$ K. However, we must consider that the temperature gradients in the Py layer in the Si/Py/NiO/Pt and in the Al_2O_3/TI/NiO/Py samples are different. The temperature gradient across the Py layer in the Si/Py/NiO/Pt sample is given by $\nabla T_{Py} \approx (K_{Si}/K_{Py})(\Delta T/t_S)$, where K_{Py} and K_{Si} are the thermal conductivities of Py and Si, and t_S is the sample thickness. For $\Delta T = 12$ K, $t_S = 0.4$ mm, $K_{Si} = 148$ W/(K m), $K_{Py} = 46.4$ W/(K m), $\nabla T_{Py} \approx 957$ K/cm. On the other hand, in the Al_2O_3/TI/NiO/Py sample, the gradient corresponding to a temperature difference ΔT is $\nabla T_{Py} \approx (K_{Al_2O_3}/K_{Py})(\Delta T/t_S)$, which gives for $\Delta T = 12$ K, $t_S = 0.5$ mm, $K_{Al_2O_3} = 41.9$ W/(K m), $\nabla T_{Py} \approx 217$ K/cm. Thus, the same $\Delta T = 12$ K would generate in the TI layer a spin current density $J_S = 7.2 \times 10^3$ A/m^2. From the data in Fig. 4(c), for $\Delta T = 12$ K, the voltage in the TI layer is $V_{SSE} = 5.9$ μV, which, for a resistance of $R = 1.08 \times 10^4$ Ω of the TI in the length of the Peltier module in a width of 1 mm, corresponds to a 2D current density of $j_C = 5.46 \times 10^{-7}$ A/m. In turn, the resistance between the Py film and the TI layer is $R \geqslant 1.0 \times 10^6$ Ω. Therefore, the resistance measurements give us assurance that the NiO layer (5 nm) is a good electrical insulator. Thus, the IEE parameter $\lambda_{IEE} = j_C/J_S$ obtained from the SSE measurements is $\lambda_{IEE} = 0.076$ nm, which is nearly the same obtained from the SPE measurements.

In summary, we have demonstrated the conversion of a spin current into a charge current in the topological insulator $(Bi_{0.22}Sb_{0.78})_2Te_3$ at room temperature, which is attributed to the inverse Edelstein effect (IEE) made possible by spin-momentum locking in the electron Fermi contours due to the Rashba field. The spin currents were generated in a thin layer of permalloy by two different processes, the spin pumping effect (SPE) and the spin Seebeck effect (SSE). In the former, we have used microwave-driven ferromagnetic resonance of the Py film to generate a spin current that is injected into the TI film in direct contact with Py. In the latter, we have used the SSE in the longitudinal configuration in Py with no contamination by the anomalous Nernst effect, which was made possible with the use of a thin NiO layer between the Py and TI layers. The results of the two measurements yield nearly identical values for the IEE coefficient, 0.076 nm, which is about twice the

value measured for the topological insulator Bi_2Se_3 (6 QL) and about four times larger than the value for $(Bi,Sb)_2Te_3$ (6 QL) [50]. Note also that the value of spin mixing conductance obtained in our work was higher than the value obtained for YIG/Bi_2Se_3-6QL ($g_{\text{eff}}^{\uparrow\downarrow} = 4.13 \times 10^{18}$ m^{-2}, as shown in the Ref. [50]). Therefore, we believe that spin transfer efficiency at the interface is one of the important aspects that enabled us to obtain a "large IEE coefficient".

This research was supported in Brazil by Conselho Nacional de Desenvolvimento Científico e Tecnológico (CNPq), Coordenação de Aperfeiçoamento de Pessoal de Nível Superior (CAPES), Financiadora de Estudos e Projetos (FINEP), Fundação de Amparo à Pesquisa do Estado de Minas Gerais (FAPEMIG), and Fundação de Amparo à Ciência e Tecnologia do Estado de Pernambuco (FACEPE). C.-Z.C. and J.S.M. acknowledge support from NSF Grants No. DMR-1207469, No. DMR-1700137, and No. DMR-0819762 (MIT MRSEC), ONR Grant No. N00014-16-1-2657, and the STC Center for Integrated Quantum Materials under NSF Grant No. DMR-1231319. C.-Z.C. is grateful for support from the startup provided by Penn State.

[1] C. Nayak *et al.*, Rev. Mod. Phys. **80**, 1083 (2008).
[2] X.-L. Qi, R. Li, J. Zang, and S.-C. Zhang, Science **323**, 1184 (2009); W. H. Campos, W. A. Moura-Melo, and J. M. Fonseca, Phys. Lett. A, **381**, 417 (2017).
[3] L. Fu and C. L. Kane, Phys. Rev. Lett. **100**, 096407 (2008).
[4] M. Z. Hasan and C. L. Kane, Rev. Mod. Phys. **82**, 3045 (2010).
[5] W. H. Campos, J. M. Fonseca, V. E. de Carvalho, J. B. S. Mendes, M. S. Rocha, and W. A. Moura-Melo, arXiv:1703.04556.
[6] X. L. Qi and S. C. Zhang, Rev. Mod. Phys. **83**, 1057 (2011).
[7] C. H. Li, O. M. J. van't Erve, J. T. Robinson, Y. Liu, L. Li, and B. T. Jonker, Nat. Nanotechnol. **9**, 218 (2014).
[8] J.-C. Rojas-Sanchez, S. Oyarzún, Y. Fu, A. Marty, C. Vergnaud, S. Gambarelli, L. Vila, M. Jamet, Y. Ohtsubo, A. Taleb-Ibrahimi, P. Le Fèvre, F. Bertran, N. Reyren, J.-M. George, and A. Fert, Phys. Rev. Lett. **116**, 096602 (2016).
[9] Y. Fan *et al.*, Nat. Nanotechnol. **11**, 352 (2016).
[10] M. I. Dyakonov and V. I. Perel, Phys. Lett. A **35**, 459 (1971).
[11] J. E. Hirsch, Phys. Rev. Lett. **83**, 1834 (1999).
[12] A. Hoffmann, IEEE Trans. Magn. **49**, 5172 (2013).
[13] S. Maekawa, H. A. Adachi, K. Uchida, J. Ieda, and E. Saitoh, J. Phys. Soc. Jpn. **82**, 102002 (2013).
[14] J. Sinova, S. O. Valenzuela, J. Wunderlich, C. H. Back, and T. Jungwirth, Rev. Mod. Phys. **87**, 1213 (2015).
[15] A. Azevedo, L. H. Vilela-Leão, R. L. Rodríguez-Suárez, A. B. Oliveira, and S. M. Rezende, J. Appl. Phys. **97**, 10C715 (2005).
[16] E. Saitoh, M. Ueda, H. Miyajima, and G. Tatara, Appl. Phys. Lett. **88**, 182509 (2006).
[17] O. Mosendz, J. E. Pearson, F. Y. Fradin, G. E. W. Bauer, S. D. Bader, and A. Hoffmann, Phys. Rev. Lett. **104**, 046601 (2010).
[18] C. W. Sandweg, Y. Kajiwara, K. Ando, E. Saitoh, and B. Hillebrands, Appl. Phys. Lett. **97**, 252504 (2010).
[19] A. Azevedo, L. H. Vilela-Leão, R. L. Rodríguez-Suárez, A. F. Lacerda Santos, and S. M. Rezende, Phys. Rev. B **83**, 144402 (2011).
[20] L. H. Vilela-Leão, C. Salvador, A. Azevedo, and S. M. Rezende, Appl. Phys. Lett. **99**, 102505 (2011).
[21] L. Liu, C.-F. Pai, Y. Li, H. W. Tseng, D. C. Ralph, and R. A. Buhrman, Science **336**, 555 (2012).
[22] C. Hahn, G. de Loubens, O. Klein, M. Viret, V. V. Naletov, and J. Ben Youssef, Phys. Rev. B **87**, 174417 (2013).
[23] M. Weiler, M. Althammer, M. Schreier, J. Lotze, M. Pernpeintner, S. Meyer, H. Huebl, R. Gross, A. Kamra, J. Xiao, Y. T. Chen, H. J. Jiao, G. E. W. Bauer, and S. T. B. Goennenwein, Phys. Rev. Lett. **111**, 176601 (2013).
[24] V. Castel, N. Vlietstra, B. J. van Wees, and J. Ben Youssef, Phys. Rev. B **90**, 214434 (2014).
[25] D. Wei, M. Obstbaum, M. Ribow, C. H. Back, and G. Woltersdorf, Nat. Commun. **5**, 3768 (2014).
[26] L. Bai, M. Harder, Y. P. Chen, X. Fan, J. Q. Xiao, and C.-M. Hu, Phys. Rev. Lett. **114**, 227201 (2015).
[27] C. Du, H. Wang, P. C. Hammel, and F. Yang, J. Appl. Phys. **117**, 172603 (2015).
[28] P. Hyde, L. Bai, D. M. J. Kumar, B. W. Southern, C.-M. Hu, S. Y. Huang, B. F. Miao, and C. L. Chien, Phys. Rev. B **89**, 180404(R) (2014).
[29] J. B. S. Mendes, R. O. Cunha, O. Alves Santos, P. R. T. Ribeiro, F. L. A. Machado, R. L. Rodríguez-Suárez, A. Azevedo, and S. M. Rezende, Phys. Rev. B **89**, 140406(R) (2014).
[30] W. Zhang, M. B. Jungfleisch, W. Jiang, J. E. Pearson, A. Hoffmann, F. Freimuth, and Y. Mokrousov, Phys. Rev. Lett. **113**, 196602 (2014).
[31] K. Ando, S. Takahashi, J. Ieda, H. Kurebayashi, T. Trypiniotis, C. H. W. Barnes, S. Maekawa, and E. Saitoh, Nat. Mater. **10**, 655 (2011).
[32] K. Ando and E. Saitoh, Nat. Commun. **3**, 629 (2012).
[33] E. Shikoh, K. Ando, K. Kubo, E. Saitoh, T. Shinjo, and M. Shiraishi, Phys. Rev. Lett. **110**, 127201 (2013).
[34] J.-C. Rojas-Sánchez *et al.*, Phys. Rev. B **88**, 064403 (2013).
[35] S. Dushenko, M. Koike, Y. Ando, T. Shinjo, M. Myronov, and M. Shiraishi, Phys. Rev. Lett. **114**, 196602 (2015).
[36] F. Bottegoni, C. Zucchetti, S. DalConte, J. Frigerio, E. Carpene, C. Vergnaud, M. Jamet, G. Isella, F. Ciccacci, G. Cerullo, and M. Finazzi, Phys. Rev. Lett. **118**, 167402 (2017).
[37] J. B. S. Mendes, S. L. A. Mello, O. Alves Santos, R. O. Cunha, R. L. Rodríguez-Suárez, A. Azevedo, and S. M. Rezende, Phys. Rev. B **95**, 214405 (2017).
[38] A. Soumyanarayanan, N. Reyren, A. Fert, and C. Panagopoulos, Nature (London) **539**, 509 (2016).
[39] Y. Ando and M. Shiraishi, J. Phys. Soc. Jpn. **86**, 011001 (2017).
[40] F. Hellman *et al.*, Rev. Mod. Phys. **89**, 025006 (2017).
[41] V. M. Edelstein, Solid State Commun. **73**, 233 (1990).
[42] E. I. Rashba, Sov. Phys. Solid State **2**, 1109 (1960).
[43] A. Manchon, H. C. Koo, J. Nitta, S. M. Frolov, and R. A. Duine, Nat. Mater. **14**, 871 (2015).

[44] K. Kondou, R. Yoshimi, A. Tsukazaki, Y. Fukuma, J. Matsuno, K. S. Takahashi, M. Kawasaki, Y. Tokura, and Y. Otani, Nat. Phys. **12**, 1027 (2016).
[45] S. Zhang and A. Fert, Phys. Rev. B **94**, 184423 (2016).
[46] J. C. Rojas Sánchez, L. Vila, G. Desfonds, S. Gambarelli, J. P. Attané, J. M. De Teresa, C. Magén, and A. Fert, Nat. Commun. **4**, 2944 (2013).
[47] J. B. S. Mendes, O. Alves Santos, L. M. Meireles, R. G. Lacerda, L. H. Vilela-Leão, F. L. A. Machado, R. L. Rodríguez-Suárez, A. Azevedo, and S. M. Rezende, Phys. Rev. Lett. **115**, 226601 (2015).
[48] Y. Shiomi, K. Nomura, Y. Kajiwara, K. Eto, M. Novak, K. Segawa, Y. Ando, and E. Saitoh, Phys. Rev. Lett. **113**, 196601 (2014).
[49] A. A. Baker, A. I. Figueroa, L. J. Collins-McIntyre, G. van der Laan, and T. Hesjedal, Sci. Rep. **5**, 7907 (2015).
[50] H. Wang, J. Kally, J. S. Lee, T. Liu, H. Chang, D. R. Hickey, K. A. Mkhoyan, M. Wu, A. Richardella, and N. Samarth, Phys. Rev. Lett. **117**, 076601 (2016).
[51] See Supplemental Material at http://link.aps.org/supplemental/10.1103/PhysRevB.96.180415 for more details about the conditions of growth, transport properties, and the crystallographic structure of the (Bi,Sb)Te films.
[52] J. Zhang *et al.*, Nat. Commun. **2**, 574 (2011).
[53] Z. Jiang, C.-Z. Chang, M. R. Masir, C. Tang, Y. Xu, J. S. Moodera, A. H. MacDonald, and J. Shi, Nat. Commun. **7**, 11458 (2016).
[54] Z. Jiang, C.-Z. Chang, C. Tang, J.-G. Zheng, J. S. Moodera, and J. Shi, AIP Adv. **6**, 055809 (2016).
[55] Y. Tserkovnyak, A. Brataas, and G. E. W. Bauer, Phys. Rev. B **66**, 224403 (2002).
[56] Y. Tserkovnyak, A. Brataas, G. E. W. Bauer, and B. I. Halperin, Rev. Mod. Phys. **77**, 1375 (2005).
[57] A. Azevedo, R. O. Cunha, F. Estrada, O. Alves Santos, J. B. S. Mendes, L. H. Vilela-Leão, R. L. Rodríguez-Suárez, and S. M. Rezende, Phys. Rev. B **92**, 024402 (2015).
[58] S. Y. Huang, W. G. Wang, S. F. Lee, J. Kwo, and C. L. Chien, Phys. Rev. Lett. **107**, 216604 (2011).
[59] A. Slachter, F. L. Bakker, and B. J. van Wees, Phys. Rev. B **84**, 020412(R) (2011).
[60] A. D. Avery, M. R. Pufall, and B. L. Zink, Phys. Rev. Lett. **109**, 196602 (2012).
[61] G. E. W. Bauer, E. Saitoh, and B. J. van Wees, Nat. Mater. **11**, 391 (2012).
[62] K. Uchida, S. Takahashi, K. Harii, J. Ieda, W. Koshibae, K. Ando, S. Maekawa, and E. Saitoh, Nature (London) **455**, 778 (2008).
[63] H. Adachi, K. Uchida, E. Saitoh, and S. Maekawa, Rep. Prog. Phys. **76**, 036501 (2013).
[64] S. R. Boona, R. C. Myers, and J. P. Heremans, Energy Environ. Sci. **7**, 885 (2014).
[65] K. Uchida, H. Adachi, T. Kikkawa, A. Kirihara, M. Ishida, S. Yorozu, S. Maekawa, and E. Saitoh, Proc. IEEE **104**, 1946 (2016).
[66] J. Holanda, O. Alves Santos, R. O. Cunha, J. B. S. Mendes, R. L. Rodríguez-Suárez, A. Azevedo, and S. M. Rezende, Phys. Rev. B **95**, 214421 (2017).
[67] H. Wang, C. Du, P. C. Hammel, and F. Yang, Phys. Rev. Lett. **113**, 097202 (2014).
[68] C. Hahn, G. de Loubens, V. V. Naletov, J. Ben Youssef, O. Klein, and M. Viret, Europhys. Lett. **108**, 57005 (2014).
[69] S. M. Rezende, R. L. Rodríguez-Suárez, and A. Azevedo, Phys. Rev. B **93**, 054412 (2016).
[70] J. Holanda, D. S. Maior, O. Alves Santos, L. H. Vilela-Leão, J. B. S. Mendes, A. Azevedo, R. L. Rodríguez-Suárez, and S. M. Rezende, Appl. Phys. Lett. **111**, 172405 (2017).